Chinese Journal of Mechanical Engineering

ORIGINAL ARTICLE

Open Access

State Estimation of Drive-by-Wire Chassis Vehicle Based on Dual Unscented Particle Filter Algorithm

Zixu Wang[1], Chaoning Chen[1], Quan Jiang[1], Hongyu Zheng[1*] and Chuyo Kaku[2]

Abstract

Accurate vehicle dynamic information plays an important role in vehicle driving safety. However, due to the characteristics of high mobility and multiple controllable degrees of freedom of drive-by-wire chassis vehicles, the current mature application of traditional vehicle state estimation algorithms can not meet the requirements of drive-by-wire chassis vehicle state estimation. This paper proposes a state estimation method for drive-by-wire chassis vehicle based on the dual unscented particle filter algorithm, which make full use of the known advantages of the four-wheel drive torque and steer angle parameters of the drive-by-wire chassis vehicle. In the dual unscented particle filter algorithm, two unscented particle filter transfer information to each other, observe the vehicle state information and the tire force parameter information of the four wheels respectively, which reduce the influence of parameter uncertainty and model parameter changes on the estimation accuracy during driving. The performance with the dual unscented particle filter algorithm, which is analyzed in terms of the time-average square error, is superior of the unscented Kalman filter algorithm. The effectiveness of the algorithm is further verified by driving simulator test. In this paper, a vehicle state estimator based on dual unscented particle filter algorithm was proposed for the first time to improve the estimation accuracy of vehicle parameters and states.

Keywords Drive-by-wire chassis vehicle, Vehicle state estimation, Dual unscented particle filter, Tire force estimation, Unscented particle filter

1 Introduction

The growing demands for flexibility, energy efficiency and safety in vehicles are driving the continuous development of intelligent transportation systems [1–3]. Among them, the drive-by-wire chassis vehicles, which with the advantages of precise knowledge of the four-wheel drive torque and independent control of the four-wheel steer angle, have become the focus of researches [4]. Simultaneously, various active safety control systems of vehicles, such as yaw stability control, lane departure avoidance system, and collision avoidance system, direct yaw moment control etc. [5–8], require accurate vehicle state information, which makes it important to accurately obtain vehicle driving state information for the safety of vehicles. The high precision wheel drive torque and the wheel steer angle information of the drive-by-wire chassis vehicle is of great significance to estimate the vehicle driving state.

At present, research on state estimation for traditional vehicles mainly based on Kalman algorithm and its derivative algorithms. Zong et al. [9, 10] used the extended Kalman filter (EKF) algorithm to measure the vehicle state to obtain the vehicle speed, and conducted offline simulation based on the actual vehicle measurement data. Zhao et al. [11] proposed

*Correspondence:
Hongyu Zheng
zhenghy@jlu.edu.cn
[1] State Key Laboratory of Automotive Simulation and Control, Jilin University, Changchun 130022, China
[2] Jiangsu Chaoli Electric Co. Ltd., Zhenjiang 212321, China

the unscented Kalman filter (UKF) algorithms to real-time observe the vehicle speed under typical operating conditions. The results show the high accuracy and robustness of the algorithm. Cui et al. [12] presented the UKF algorithm to estimate lateral tire force, tire slip angle, vehicle sideslip angle and road friction coefficient, UKF estimator was accurate in different road conditions. Aiming at the vehicle lateral velocity estimation method (VLVEM), Zhang et al. [13] derived a stack bidirectional long short-term memory (SBi-LSTM) algorithm based on the federated Kalman filter (FKF) algorithm proved by simulations that has the characteristics of accurate estimation, robustness and fault tolerance. Zhang et al. [14] proposed an adaptive treble extend Kalman filter and designed a sliding mode update, which made the overall system become more robust for tire force estimation. The results showed the algorithm achieved an excellent performance in a vertical force evaluation.

On the other hand, the particle filter algorithm does not require the assumption of Gaussian distribution and has the advantage of being able to deal with high-order nonlinear problems. Therefore, it has begun to be applied in the research of vehicle state estimation. Lenzo et al. [15] investigated a particle filter (PF) approach to estimate the chassis sideslip angle of road vehicle, and the results showed satisfactory performance of the algorithm. However, the PF algorithm also has the disadvantages of slow convergence speed and large computational requirements [16]. Ko et al. [17] compared the performance of PF and EKF in the position estimation of underwater robots and pointed out that the result of PF is smoother and more stable, but the calculation speed is slower. Furthermore, the general PF also has: (1) Particle degradation: After multiple sampling, the particles will be concentrated near the higher probability density value, causing the update invalid; (2) sample size dependence: There is a strong conflict between particle filter calculation efficiency and calculation accuracy. If the number of particles is insufficient, the estimation result would be distorted [18]. Berntorp [19] compared the time average root mean square error probability of different particle numbers in the research and illustrated that the number of particles is inversely proportional to the measurement error.

To address the aforementioned issues, some researchers combined Kalman and its derivative filtering theory with PF. For example, the unscented particle filter (UPF) algorithm is based on the particle filter framework and uses the algorithm of UKF to generate the importance function, which incorporates the latest observational information into prior update. Liu et al. [20] proposed a UPF with fine resampling to estimate tire slip angle and yaw rate, the simulation proved its higher robustness compared to the UKF, and with smaller fluctuation in error value compared to the sequential importance resampling particle filter (SIR-PF). Aiming at improving the accuracy of vehicle positioning, Lin et al. [21] employed a particle-assisted unscented Kalman filter (PAUKF), in which UKF algorithm updates the vehicle state and PF algorithm to provide additional positioning information. Liu et al. [22] presented a road friction coefficient estimation method that combines the auxiliary particle filter and the iterative extended Kalman filter (APF-IEKF), which used the iterative algorithm to process the results of the first step, the simulation and experiment results in low tire road coefficient (snow course) in winter were provided to demonstrate the accuracy and efficiency of the proposed approach.

Current research on the state estimation problem of the drive-by-wire chassis vehicle is primarily based on Kalman and PF as well as the derivative algorithm. Song et al. [23] built a chassis controller for the direct yaw moment control (DYC) system of a four-wheel independent steer (4WIS) vehicle, which utilized the UKF estimation of the vehicle tire slip angle, longitudinal speed and tire force. Chu et al. [24] applied the UPF algorithm to estimate the lateral tire force, longitudinal velocity, lateral velocity and yaw rate of the in-wheel-motor vehicle, verifying its effectiveness and robustness. Zhu et al. [25] proposed an improved particle filter to estimate the state parameters of in-wheel-motor vehicle under complex noise and sensor failure conditions, and the simulation results showed that its performance is superior to UPF and UKF observers.

Because the drive-by-wire chassis vehicle has the advantages of drive torque and steer angle parameters accurate controllability, it is considered to use two observers to process different state vectors, and to observe the vehicle state parameters in cooperation with each other. Such an algorithm structure reduces parameter uncertainty and interference caused by model parameter changes, thereby improving the accuracy of the observed measurement. Pei et al. [26] presented a joint estimation method of vehicle state and parameters based on dual unscented Kalman filter (DUKF), which exhibited high estimation accuracy for the vehicle state and parameters of an 8×8 distributed electric vehicle. Wang et al. [27] designed a combination of UKF and EKF algorithm for the estimation of tire sideslip angles in a four-wheel independent drive (4WID) electric vehicle and a hybrid estimator was formed with strong robustness through the use of weighting factors.

In this paper, a dual unscented particle filter (DUPF) algorithm is proposed to estimate the driving state parameters of the drive-by-wire chassis vehicle. The main contributions of this article are as follows:

1. For the first time, the DUPF algorithm is utilized to estimate the driving state of the drive-by-wire chassis vehicle, which reduces the uncertainty of the parameters and the influence of the model parameter changes on the estimation results during the driving process. Consequently, the accuracy of the vehicle state parameters and the robustness of the algorithm were improved.
2. The DUPF algorithm makes full use of the characteristics of easy acquisition of the parameters of the drive-by-wire chassis, combined with low-cost sensors, which can estimate various state information and parameter information of the vehicle, and has a wide range of applications.
3. It is verified by simulation experiments that the DUPF algorithm has higher estimation accuracy than the UKF algorithm in the double line change (DLC), weave test and cornering brake test. The DUPF algorithm is proved to have a good prospect in practical applications in the HIL test.

The rest of this article is structured as follows: Section 2 introduces a nonlinear drive-by-wire chassis vehicle model and Pacejka tire model. Section 3 introduces the DUPF algorithm that used for vehicle state and parameter estimation. Section 4 introduces the simulation and driving simulator test under the DLC and weave test. Section 5 makes a conclusion of this article.

2 Models and Estimation Algorithm

2.1 Drive-by-Wire Chassis Vehicle Dynamic Model

As shown in Figure 1, α_{ij} is the wheel slip angle, δ_{ij} is the wheel steer angle (i can be l and r represent left and right;j can be f and r represent front and rear), Vx, Vy are the longitudinal velocity and lateral velocity of the center of mass of the vehicle in the body coordinate system, a_x, a_y are the longitudinal acceleration and lateral acceleration of the center of mass of the vehicle in the body coordinate system, β is the slip angle of the center of mass, θ is the wheel forward direction angle.

Wheel slip angle can be expressed as:

$$\alpha_{ij} = -\delta_{ij} + \theta_{ij}. \tag{1}$$

The vehicle state parameter estimator proposed in this paper is based on a nonlinear drive-by-wire chassis vehicle dynamics model, which contains three degrees of freedom in the longitudinal, lateral and yaw directions. F_{xij}, F_{yij} represent the longitudinal and lateral tire force in the wheel coordinate system. X_{ij}, Y_{ij} are the longitudinal component force and the lateral component force received at the center of the wheel in the body coordinate system as:

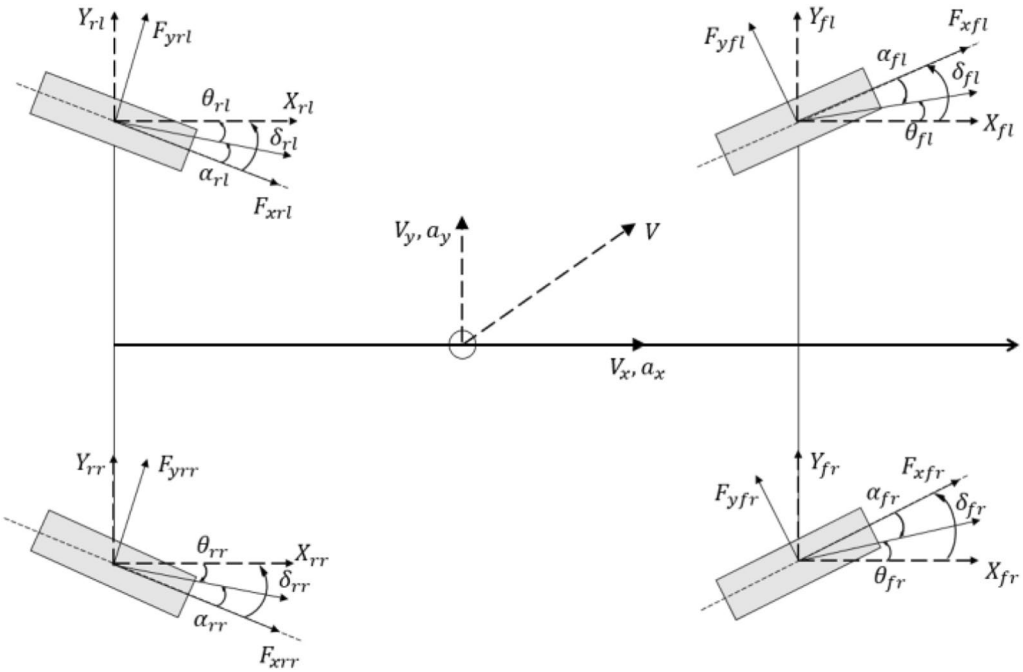

Figure 1 Drive-by-wire chassis vehicle dynamic model

$$\begin{bmatrix} X_{ij} \\ Y_{ij} \end{bmatrix} = R(\delta_{ij}) \begin{bmatrix} F_{x\_ij} \\ F_{y\_ij} \end{bmatrix} = \begin{bmatrix} \cos\delta_{ij} & -\sin\delta_{ij} \\ \sin\delta_{ij} & \cos\delta_{ij} \end{bmatrix} \begin{bmatrix} F_{x\_ij} \\ F_{y\_ij} \end{bmatrix}. \tag{2}$$

In addition to the tire force, the air resistance experienced by the vehicle during driving is:

$$F_d = \frac{1}{2}\rho C_d A v_x^2, \tag{3}$$

where ρ is the air density, C_d is the drag coefficient, A is the frontal area. Therefore, the motion equations of the vehicle in the longitudinal, lateral and yaw directions are:

$$\begin{cases} ma_x = m(\dot{V}_x - \dot{\varphi} V_y) = \sum_{i=l}^{r}\sum_{j=f}^{r} X_{ij} - F_d, \\ ma_y = m(\dot{V}_y - \dot{\varphi} V_x) = \sum_{i=l}^{r}\sum_{j=f}^{r} Y_{ij}, \\ I_z\ddot{\varphi} = \frac{t}{2}(-X_{lf} + X_{rf} - X_{lr} + X_{rr}) \\ \quad + l_f(Y_{lf} + Y_{rf}) - l_r(Y_{lr} + Y_{rr}), \end{cases} \tag{4}$$

where $\dot{\varphi}$ is the yaw rate, l_f, l_r are the distance from the center of mass to the front axle and rear axle. In the case of considering wheel load transfer, the vertical loads of each wheel are:

$$\begin{cases} F_{zlf} = \frac{mgl_r}{2(l_f+l_r)} - \frac{m_s a_x h_s}{2(l_f+l_r)} - \frac{m_s a_y h_s}{t_f}, \\ F_{zrf} = \frac{mgl_r}{2(l_f+l_r)} - \frac{m_s a_x h_s}{2(l_f+l_r)} + \frac{m_s a_y h_s}{t_f}, \\ F_{zlr} = \frac{mgl_f}{2(l_f+l_r)} + \frac{m_s a_x h_s}{2(l_f+l_r)} - \frac{m_s a_y h_s}{t_r}, \\ F_{zrr} = \frac{mgl_f}{2(l_f+l_r)} + \frac{m_s a_x h_s}{2(l_f+l_r)} + \frac{m_s a_y h_s}{t_r}, \end{cases} \tag{5}$$

where m_s is the sprung mass, h_s is the height of the mass center of the sprung mass. The sideslip angle β can be calculated by longitudinal velocity and lateral velocity:

$$\beta = \arctan\left(\frac{V_y}{V_x}\right). \tag{6}$$

2.2 Pacejka Tire Model

As an important part of the direct contact between the vehicle and ground, the functional relationship between the tire force and tire motion parameters is the basis of the vehicle dynamics research. The commonly used tire models are mainly divided into three categories: Physical models, empirical and semi-empirical models, and finite element models. Each tire model has its own advantages and disadvantages. In this paper, the Pacejka tire model is selected, and the model calculation formula is [28]:

$$y = D\sin\{C\arctan[Bx - E(Bx - \arctan Bx)]\}, \tag{7}$$

where y is the lateral tire force, x is the tire slip angle, B is the stiffness coefficient, C is the shape coefficient, D is the maximum point, E is the curvature coefficient. The forward direction angle of each wheel can be obtained through tire kinematics:

$$\begin{bmatrix} \theta_{lf} \\ \theta_{rf} \\ \theta_{lr} \\ \theta_{rr} \end{bmatrix} = \begin{bmatrix} \arctan\left(\frac{V_y+\dot{\varphi}l_f}{V_x-\dot{\varphi}t/2}\right) \\ \arctan\left(\frac{V_y+\dot{\varphi}l_f}{V_x+\dot{\varphi}t/2}\right) \\ \arctan\left(\frac{V_y-\dot{\varphi}l_f}{V_x-\dot{\varphi}t/2}\right) \\ \arctan\left(\frac{V_y-\dot{\varphi}l_f}{V_x+\dot{\varphi}t/2}\right) \end{bmatrix}. \tag{8}$$

Then the vertical load of the tire can be solved according to Eq. (5), the tire slip angle can be obtained from Eq. (1) and Eq. (8), then the tire cornering force can be obtained.

3 Dual Unscented Particle Filter Algorithm

In the DUPF algorithm, two UPF observers operate separately and simultaneously. In this paper, the vehicle state estimator and the vehicle parameter estimator exchange and correct information with each other. Both UPF observers are composed of particle sampling, UT transformation, prediction update, and calculate weight resampling. The principle of DUPF is shown in Figure 2.

After discretizing the dynamic model of the vehicle and selecting the state vector and parameter vector, a vehicle state estimator based on the DUPF algorithm can be realized. The number of Sigma points depend on the number of state vectors and parameter vectors. In the DUPF algorithm, the vehicle dynamics model provides control variables, including each wheel torque, steer angle, wheel angular velocity and angular acceleration.

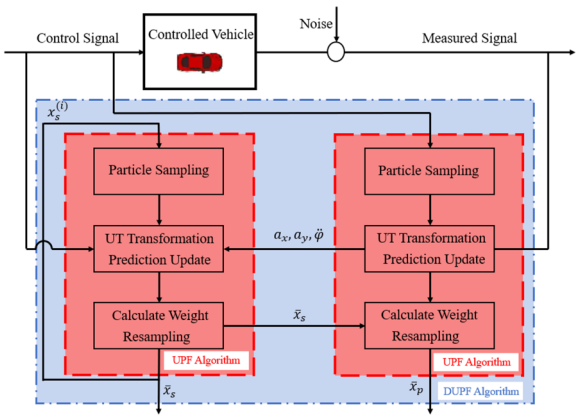

Figure 2 DUPF state observer algorithm logic diagram

The DUPF algorithm returns the observed vehicle yaw rate, vehicle longitudinal and lateral acceleration to the vehicle model.

3.1 Unscented Particle Filter Observer Design

In this research, only the movement of the vehicle on the horizontal plane is considered. Based on the movement information of the vehicle in the longitudinal, lateral and yaw directions, the vehicle state is set to x_s, which is serves as the observation vector for the DUPF observer:

$$x_s = \left[\begin{array}{cccccc} V_x & V_y & \dot{\varphi} & a_x & a_y & \ddot{\varphi} \end{array}\right]^{\mathrm{T}}. \tag{9}$$

The vehicle parameter vector x_p is:

$$x_p = \left[\begin{array}{cccccccc} F_{xlf} & F_{xrf} & F_{xlr} & F_{xrr} & F_{ylf} & F_{yrf} & F_{ylr} & F_{yrr} \end{array}\right]^{\mathrm{T}}. \tag{10}$$

Among them, F_{xij}, F_{yij} respectively represent the longitudinal tire force and lateral tire force. Because the wheel steer angle and wheel driving torque signals of the drive-by-wire chassis vehicle can be directly obtained, the input vector of the observer is as follows:

$$u = \left[\begin{array}{cccc} T_{wij} & \delta_{ij} & \omega_{ij} & \dot{\omega}_{ij} \end{array}\right]^{\mathrm{T}}. \tag{11}$$

The observation vector is:

$$y = \left[\begin{array}{ccc} \dot{\varphi} & a_x & a_y \end{array}\right]. \tag{12}$$

Thus, there is the system discrete equations:

$$x_s(k+1) = f_s\left[x_s(k), x_p(k), u(k)\right] + Q_s(k), \tag{13}$$

$$y_s(k) = H_s x_s + v(k), \tag{14}$$

$$H_s = \left[\begin{array}{cccccc} 0 & 0 & 1 & 0 & 0 & 0 \\ 0 & 0 & 0 & 1 & 0 & 0 \\ 0 & 0 & 0 & 0 & 1 & 0 \end{array}\right], \tag{15}$$

$$x_p(k+1) = f_p[x_s(k), u(k)] + Q_p(k), \tag{16}$$

$$y_p(k+1) = h_p\left[x_p(k+1), u(k+1)\right] + R(k+1), \tag{17}$$

where, Q_s and Q_p, represent the process noise in Eq. (13) and Eq. (16) respectively. v, R represent the measurement noise in Eq. (14) and Eq. (17) respectively, and Q_s, Q_p, R are the diagonal matrixes.

$$\begin{cases} V_x(k+1) = V_x(k) + \Delta T a_x(k), \\ V_y(k+1) = V_y(k) + \Delta T a_y(k), \\ \dot{\varphi}(k+1) = \dot{\varphi}(k) + \Delta T \ddot{\varphi}. \end{cases} \tag{18}$$

Extract N particles $\left\{x_{s0}^{(i)}\right\}_{i=1}^{N}, \left\{x_{p0}^{(i)}\right\}_{i=1}^{N}$ from the prior distribution $p_s(x_{s0}), p_p(x_{p0})$ respectively. Obtain the initial value of the state vectors $x_{s0}^{(i)}, x_{p0}^{(i)}$ and the initial covariance of the state vectors: $P_{s0}^{(i)}, P_{p0}^{(i)}$ respectively. The initial value and initial covariance of the state vectors can be correspondingly expressed by:

$$\bar{x}_s^{(i)}(0) = E\left[x_s^{(i)}(0)\right], \tag{19}$$

$$P_s^{(i)}(0) = E\left[\left(x_s^{(i)}(0) - \bar{x}_s^{(i)}(0)\right)\left(x_s^{(i)}(0) - \bar{x}_s^{(i)}(0)\right)^{\mathrm{T}}\right]. \tag{20}$$

Calculate the Sigma point set:

$$\begin{cases} x_s^{(i)a}(k-1) = \left[\begin{array}{c} \bar{x}_s^{(i)a}(k-1) \\ \bar{x}_s^{(i)a}(k-1) \pm \sqrt{(n_a+\lambda_s)P_s^{(i)a}(k-1)} \end{array}\right]^{\mathrm{T}}, \\ x_p^{(i)a}(k-1) = \left[\begin{array}{c} \bar{x}_p^{(i)a}(k-1) \\ \bar{x}_p^{(i)a}(k-1) \pm \sqrt{(n_a+\lambda_p)P_p^{(i)a}(k-1)} \end{array}\right]^{\mathrm{T}}, \end{cases} \tag{21}$$

$$\lambda = \alpha^2(n+\kappa) - n, \tag{22}$$

$$\begin{cases} W_0^{(m)} = \lambda/(L+\lambda), \\ W_i^{(m)} = \lambda/2(L+\lambda), \end{cases} i = 1, 2, ..., 2L, \tag{23}$$

$$\begin{cases} W_0^{(c)} = \lambda/(L+\lambda) + \left(1-\alpha^2+\beta\right), \\ W_i^{(c)} = \lambda/2(L+\lambda), \end{cases} i = 1, 2, ..., 2L, \tag{24}$$

where $\kappa = 0$, $\alpha = 0.001$, $\beta = 2$. After updating the Sigma point, $x_s^{(i)x}$ and $x_p^{(i)x}$ can be explained as follows:

$$x_s^{(i)x}\left(k|k-1\right) = f_s\left[x_s^{(i)x}(k-1), \hat{x}_p^{(i)}(k-1), u(k-1)\right], \tag{25}$$

$$x_p^{(i)x}\left(k|k-1\right) = f_h\left[x_s^{(i)}(k-1), u(k-1)\right]. \tag{26}$$

Then the predicted value of the state vector x_s, x_p obtained by weighted calculation is:

$$\bar{x}_s^{(i)}\left(k|k-1\right) = \sum_{j=0}^{2n_s} W_{s,j}^{(m)} x_{s,j}^{(i)x}\left(k|k-1\right), \tag{27}$$

$$\bar{x}_p^{(i)}\left(k|k-1\right) = \sum_{j=0}^{2n_p} W_{p,j}^{(m)} x_{p,j}^{(i)x}\left(k|k-1\right). \tag{28}$$

Linear and non-linear changes are made to the Sigma point, and the system predicted values and covariance predicted values are as follows:

$$\bar{y}_s^{(i)}(k|k-1) = \sum_{j=0}^{2n_s} W_{s,j}^{(m)} y_s^{(i)x}(k|k-1), \tag{29}$$

$$P_{s(x,x)}^{(i)}(k|k-1) = \sum_{j=0}^{n_s} W_{s,j}^{(c)} \left[x_{s,j}^{(i)}(k|k-1) - \bar{x}_s^{(i)}(k|k-1)\right] \left[x_{s,j}^{(i)}(k|k-1) - \bar{x}_s^{(i)}(k|k-1)\right]^{\mathrm{T}}. \tag{30}$$

The updated filter gain matrix is:

$$K_s(k) = P_{s(x,y)}(k)\left[P_{s(\tilde{y},\tilde{y})}\right]^{-1}. \tag{31}$$

Then there are posterior estimates and posterior variance:

$$\bar{x}_s^{(i)}(k) = \bar{x}_s^{(i)}(k|k-1) + K_s(k)\left[y_s(k) - \bar{y}_s^{(i)}(k|k-1)\right], \tag{32}$$

$$\hat{P}_s^{(i)}(k) = P_{s(x,x)}^{(i)}(k|k-1) - K_s(k)P_{s(\tilde{y},\tilde{y})}(k)[K_s(k)]^{\mathrm{T}}. \tag{33}$$

Furthermore, $\widehat{x}_p^{(i)}(k)$, $\widehat{P}_p^{(i)}(k)$ can be obtained by the same method.

For each particle:

$$\begin{aligned}\hat{x}_s^{(i)}(k) &\sim q\left(\hat{x}_s^{(i)}(k)\middle|x_s^{(i)}(0:k-1), y_s(1:k)\right)\\ &= N\left(\bar{x}_s^{(i)}(k), \hat{P}_s^{(i)}(k)\right),\end{aligned} \tag{34}$$

$$\hat{x}_s^{(i)}(0:k) \triangleq \left(x_s^{(i)}(0:k-1), \hat{x}_s^{(i)}(k)\right). \tag{35}$$

The weight of each particle is:

$$\omega_s^{(i)}(k) \propto \frac{p\left(y_s(k)\middle|\hat{x}_s^{(i)}(k)\right)p\left(\hat{x}_s^{(i)}(k)\middle|x_s^{(i)}(k-1)\right)}{q\left(\hat{x}_s^{(i)}(k)\middle|x_s^{(i)}(0:k-1), y_s(1:k)\right)}. \tag{36}$$

Particle normalization:

$$\tilde{\omega}_s^{(i)}(k) = \omega_s^{(i)}(k) \Big/ \sum_{j=1}^{N} \omega_s^{(j)}(k). \tag{37}$$

3.2 Resampling

After multiple iterations, most of the particle weights in the PF algorithm will approach 0. It is necessary to replicate high-weight particles through resampling and eliminate low-weight particles. Recording the weights of each particle as:

$$\omega_s^{(i)}(k) = 1/N. \tag{38}$$

Therefore, the output state vector is:

$$\hat{x}_s^{(i)}(k) = \sum_{i=1}^{N} \omega_s^{(i)}(k)\bar{x}_s^{(i)}(k), \tag{39}$$

$$\hat{P}_s(k) = \sum_{i=1}^{N} \omega_s^{(i)}(k)\left[x_s^{(i)}(k) - \bar{x}_s^{(i)}(k)\right]\left[x_s^{(i)}(k) - \bar{x}_s^{(i)}(k)\right]^{\mathrm{T}}. \tag{40}$$

The same method can be used to obtain $\widehat{x}_p^{(i)}(k)$, $\widehat{P}_p(k)$.

Table 1 Factors and their levels

Parameters	Variance
Longitudinal acceleration	10^{-3}
Lateral acceleration	10^{-3}
Yaw rate	10^{-5}
Drive torque	1
Wheel speed	10^{-3}
Wheel angular acceleration	10^{-3}
Wheel steer angle	5×10^{-7}

Table 2 Parameters of the tested vehicle

Parameters (unit)	Value
Vehicle mass (kg)	930
Moment of inertia (kg·m^2)	1460
Center of mass height (m)	0.54
Distance from center of mass to front axle (m)	1.103
Distance from center of mass to rear axle (m)	1.244
Wheelbase (m)	1.4
Drag coefficient	0.3
Frontal area (m^2)	1.6

4 Simulation and Results

Drive-by-wire chassis vehicles can achieve special working conditions such as U-turn or wedge driving in place, but the driving speed under these working conditions is usually low, which can be verified by common kinematic models. Therefore, through MATLAB/Simulink CarSim simulation, the DUPF algorithm is verified under DLC, weave test and cornering brake test. The DUPF algorithm used here is implemented in the MATLAB/Simulink. The response of the CarSim vehicle simulation model is taken as a

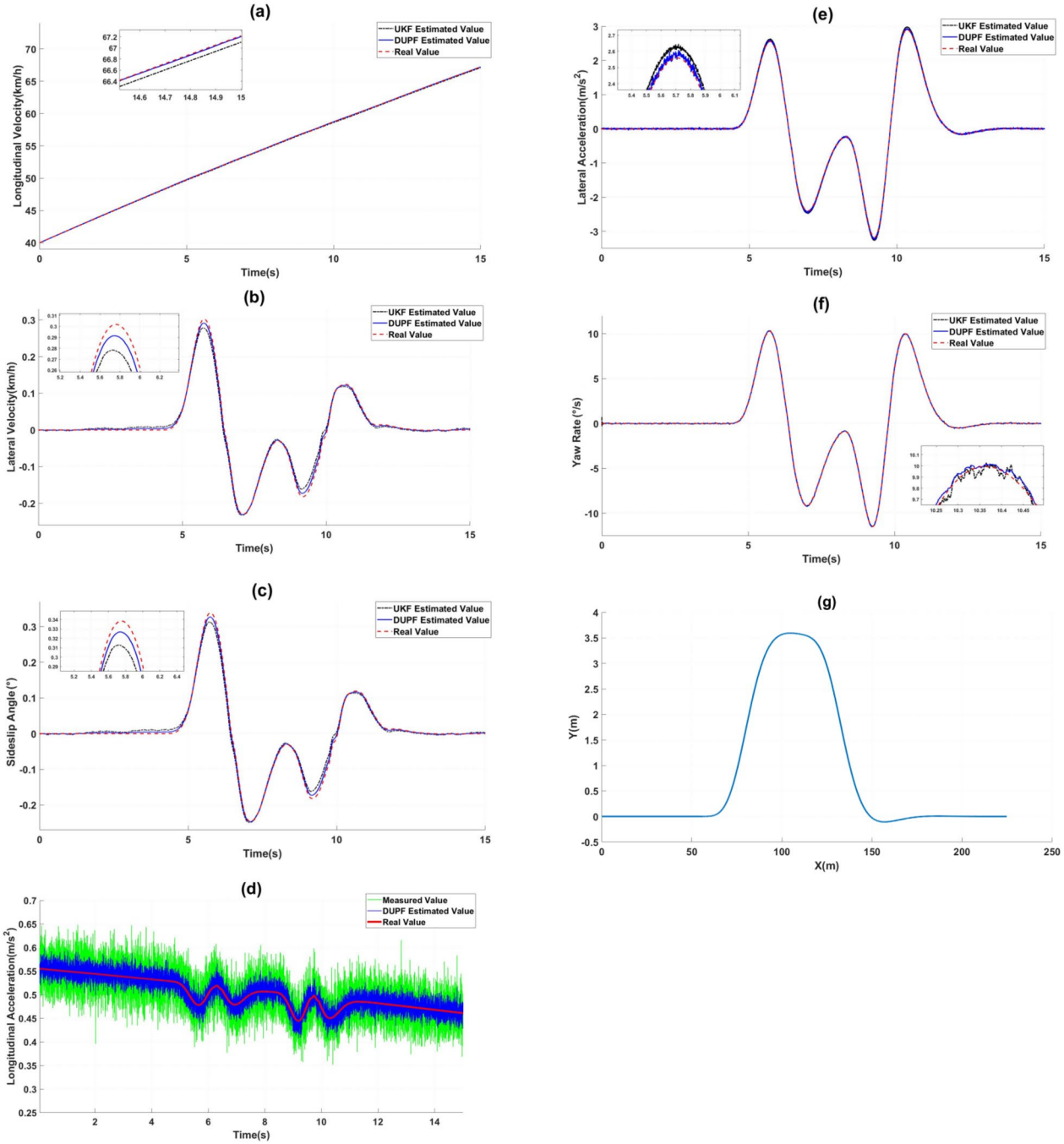

Figure 3 DUPF algorithm estimation result in DLC: (**a**) Longitudinal velocity, (**b**) Lateral velocity, (**c**) Vehicle sideslip angle, (**d**) Longitudinal acceleration, (**e**) Lateral acceleration, (**f**) Yaw rate, (**g**) Driving path

reference or measured state to evaluate the performance of the proposed DUPF algorithm. In order to simulate the real signal of the sensor, in the CarSim sensor output port, noise signals are added for the gyroscope longitudinal acceleration, lateral acceleration, yaw rate, wheel drive torque, wheel speed, wheel angular acceleration and wheel steer angle. The type of noise is Gaussian noise. The details of the noise signal are shown in Table 1. The vehicle parameters used in the tested vehicle are shown in Table 2.

Table 3 Calculated value of vehicle parameter TASE under DLC

Calculated parameters	DUPF	UKF
Yaw rate	1.6894	2.0084
Longitudinal velocity	0.6290	4.9872
Lateral acceleration	0.3572	1.3962
Lateral velocity	0.0442	0.2015
Sideslip angle	0.0262	0.1347

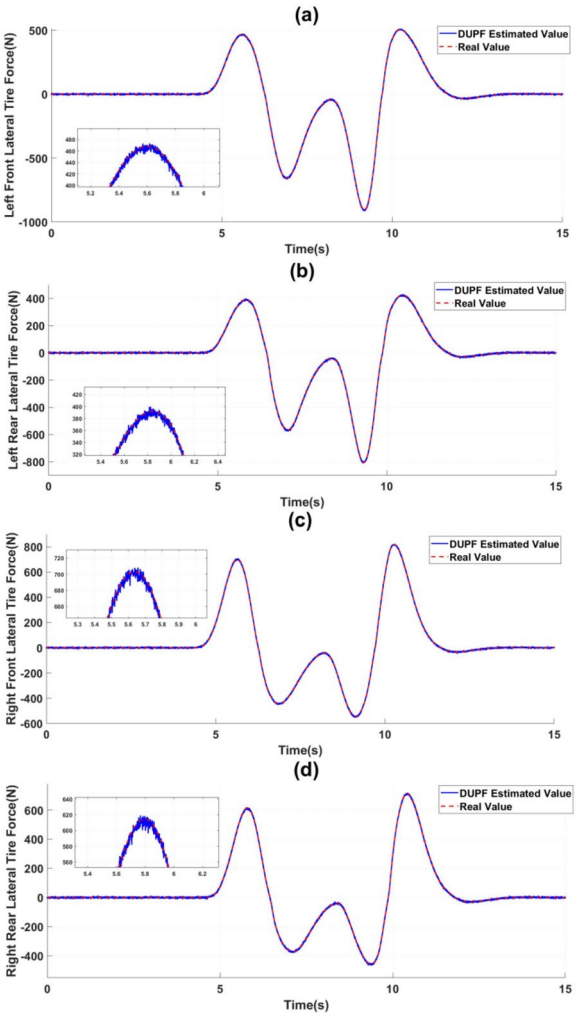

Figure 4 DUPF algorithm estimation result in DLC: (**a**) Left front lateral tire force, (**b**) Left rear lateral tire force, (**c**) Right front lateral tire force, (**d**) Right rear lateral tire force

4.1 DLC Simulation

In order to verify the estimation effect of the DUPF algorithm in the longitudinal and lateral directions, a variable-speed DLC is designed. The initial speed is 40 km/h, the output torque of each wheel is 41 N · m. The initial value of the vehicle driving state variable is $x_s(0) = \left[40/3.6\ 0\ 0\ 0\ 0\ 0\right]^{\mathrm{T}}$. The initial value of the tire force parameter variable is $x_p(0) = \left[0\ 0\ 0\ 0\ 0\ 0\right]^{\mathrm{T}}$. The road friction coefficient is 0.85.

Currently, the EKF algorithm and the UKF algorithm are relatively mature and widely used techniques for vehicle state estimation. The performances of the two algorithms are relatively close when dealing with the problem of vehicle state estimation [16]. However, because the UKF algorithm linearizes the posterior estimation, it achieves better performance for systems with fast or rapid state change. Therefore, this paper selects the UKF algorithm and DUPF algorithm for comparison. To verify the effectiveness of the algorithm, a vehicle state estimator designed by the commonly used UKF algorithm is introduced for comparison.

Figure 3 shows the vehicle state observation results obtained by the DUPF and UKF observers. In the longitudinal direction, both methods are relatively accurate in estimating the longitudinal vehicle velocity. However, as the vehicle velocity increases, the estimation accuracy of the DUPF algorithm remains high, while the error of the UKF algorithm is slightly higher than that of the DUPF algorithm. In terms of the longitudinal acceleration of the vehicle, it can be observed that the DUPF algorithm exhibits a filtering effect on the longitudinal acceleration of the vehicle. In terms of vehicle lateral state estimation, as the vehicle velocity increases, the lateral excitation increases, resulting in an increase in the errors of both estimation algorithms. The estimation errors of the sideslip angle, lateral velocity, and lateral acceleration gradually increase. However, the estimation error of the DUPF algorithm is smaller than that of the UKF algorithm.

In order to illustrate the advantages of the DUPF algorithm more intuitively, the time-average square error (TASE) is used as a reference indicator in Ref. [29] . TASE can be utilized to visualize and compare the estimated performance of the proposed method and existing methods at each Monte Carlo run.

$$TASE = \frac{1}{T}\sum_{k=1}^{T}\left(x_k^s - \hat{x}_k^s\right)^2, s = 1, ..., M, \tag{41}$$

where x_k^s and $\widehat{x}_k^s$ represent the reference vector and the estimated vector in the sth Monte Carlo, respectively. In this paper, only the TASE results of the DUPF algorithm and the UKF algorithm are compared to further quantify the accuracy of the DUPF algorithm. That is, x_k^s is the real value of the sensor at time k, and $\widehat{x}_k^s$ is the estimated value of the DUPF algorithm and the UKF algorithm at time k.

As shown in Table 3, the estimation results of the DUPF algorithm exhibit better accuracy compared to the

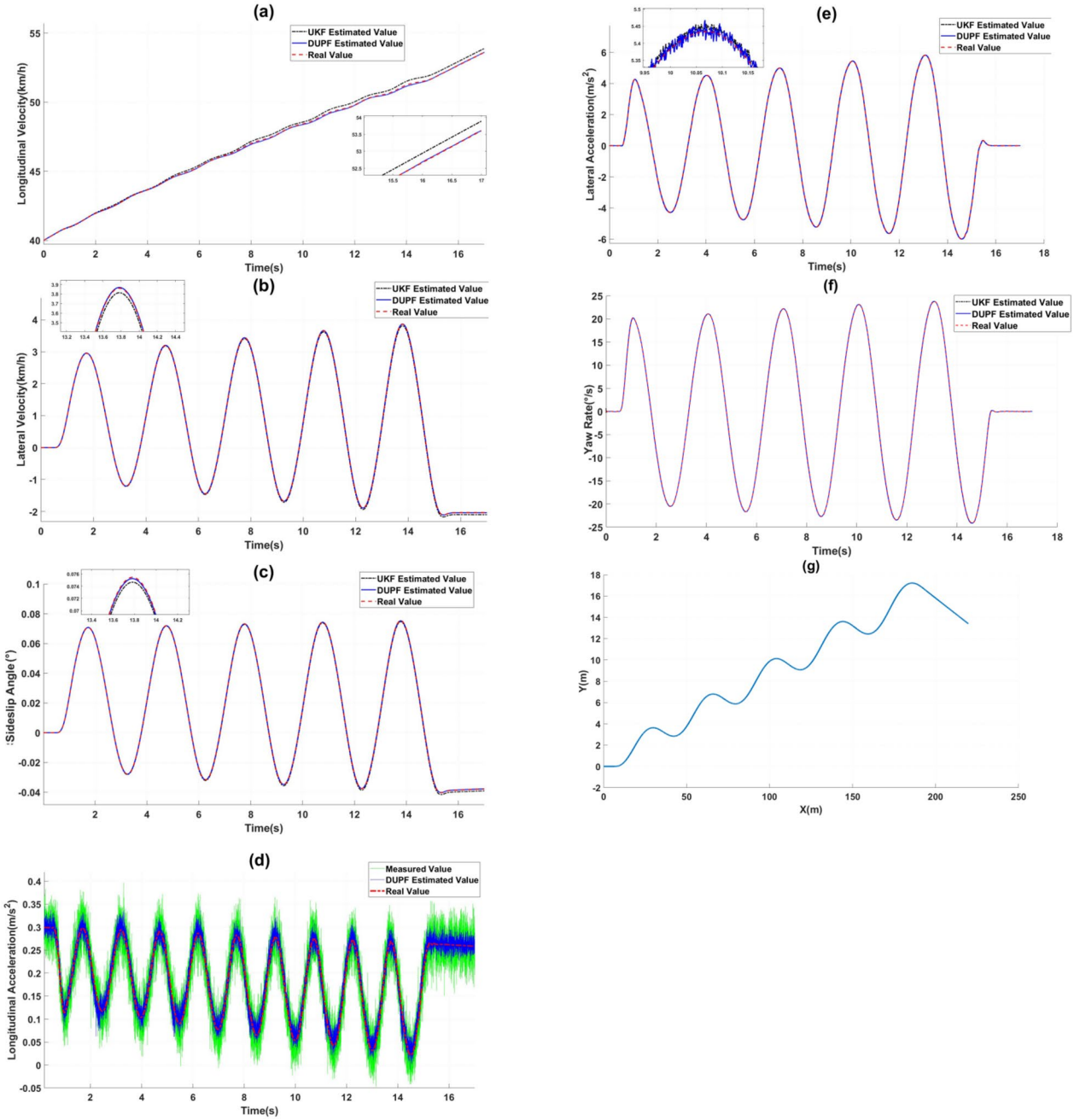

Figure 5 DUPF algorithm estimation result in weave test: (**a**) Longitudinal velocity, (**b**) Lateral velocity, (**c**) Vehicle sideslip angle, (**d**) Longitudinal acceleration, (**e**) Lateral acceleration, (**f**) Yaw rate, (**g**) Driving path

UKF algorithm. The DUPF algorithm has 15.88%−87.38% advantage.

As shown in Figure 4, because the known drive torque of each wheel of the drive-by-wire chassis vehicle, the estimation result obtained by the DUPF algorithm is closer to the true value of the CarSim output, resulting in a low error in the estimation of tire lateral force.

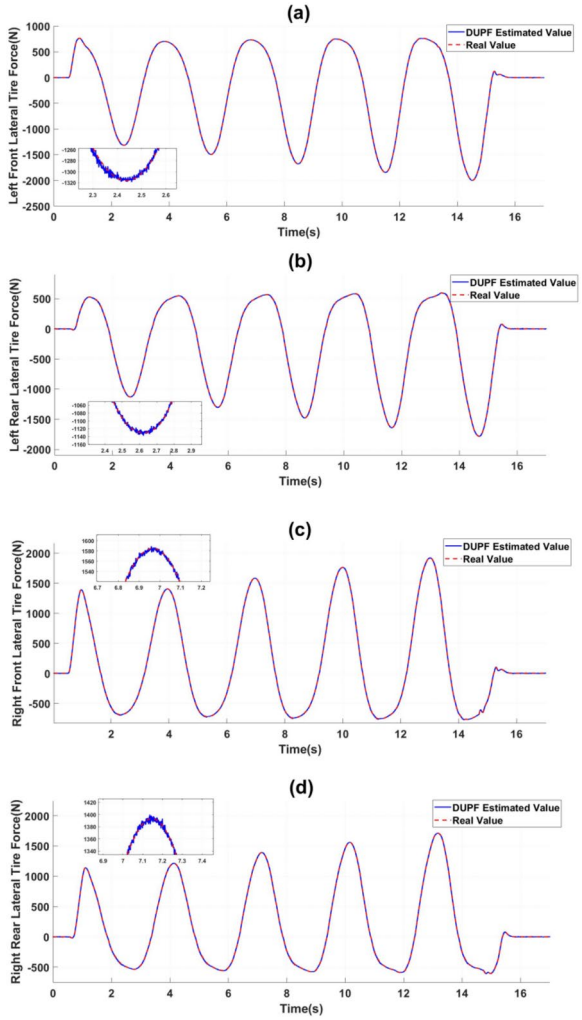

Figure 6 DUPF algorithm estimation result in weave test: (**a**) Left front lateral tire force, (**b**) Left rear lateral tire force, (**c**) Right front lateral tire force, (**d**) Right rear lateral tire force

4.2 Weave Test

To further verify the accuracy of the algorithm's observation in the lateral state, a weave test was set. In the weave test, the road friction coefficient is set as 0.85, the wheel steer angle changes with time as a sinusoidal open-loop control, and the output torque of the four wheels is set as 25 N·m. To prevent the vehicle from sideslip during the process of turning while accelerating at high velocity, a simulation time of 17 s was set. This working condition also used a vehicle state observer based on UKF algorithm, which was compared to the DUPF vehicle state observer.

Figure 5 displays the estimated vehicle driving state under weave test. In the longitudinal direction, the estimation of longitudinal velocity by the two methods is relatively accurate within 0–5 s. However, as the vehicle longitudinal velocity increases, the estimation accuracy of the DUPF algorithm remains high between 5–17 s, and the error of the UKF algorithm is significantly higher than that of DUPF algorithm. According to the longitudinal acceleration of the vehicle, it can be found that the DUPF algorithm still exhibits a significant filtering effect on the longitudinal acceleration of the vehicle under weave test. In terms of vehicle lateral state estimation, as the vehicle velocity increases, the lateral excitation increases, resulting in an increase in the errors of both estimation algorithms. There is a certain value error between the lateral velocity and sideslip angle estimated by the UKF algorithm at 15–17 s and the actual value of the CarSim output. The main reason is the inclusion of an integral term in the velocity estimation process, resulting in a deviation, which can be corrected under appropriate conditions through sensors or GPS and other sensors. However, this paper will not introduce such corrections. The vehicle state observer based on the DUPF algorithm and UKF algorithm exhibit low error between the estimated results and the true values such as lateral acceleration and yaw rate thereby demonstrating the superior performance and robustness of the DUPF algorithm.

Figure 6, shows the estimation result of the lateral tire force under the condition of variable velocity weave test. It can be observed that the observation result of the lateral force of the vehicle by DUPF is consistent with the actual output value of CarSim.

4.3 Cornering Brake Test

To demonstrate the effectiveness of the DUPF algorithm under braking, a cornering braking condition is established. The initial velocity of the vehicle is 70 km/h, the vehicle braking system exerts a pressure of 0.7 MPa on the brake disc at 0 s, and the steering wheel angle is 30°. The simulation time is 5 s.

Figure 7 displays the estimated result of the vehicle's driving state under the cornering braking test. In the vehicle braking state, both the DUPF algorithm and the UKF algorithm exhibit a certain error in the velocity estimation of the vehicle, but the error value of the DUPF algorithm is smaller than that of the UKF algorithm. On the other hand, both the DUPF algorithm and the UKF algorithm are accuratly estimate the lateral and longitudinal acceleration of the vehicle, but the estimated value of the DUPF algorithm is relatively stable.

Figure 8 displays the estimated result of the lateral force of the four wheels of the vehicle under the condition of turning braking. The DUPF algorithm accurately estimates the tire lateral force, and is suitable for solving

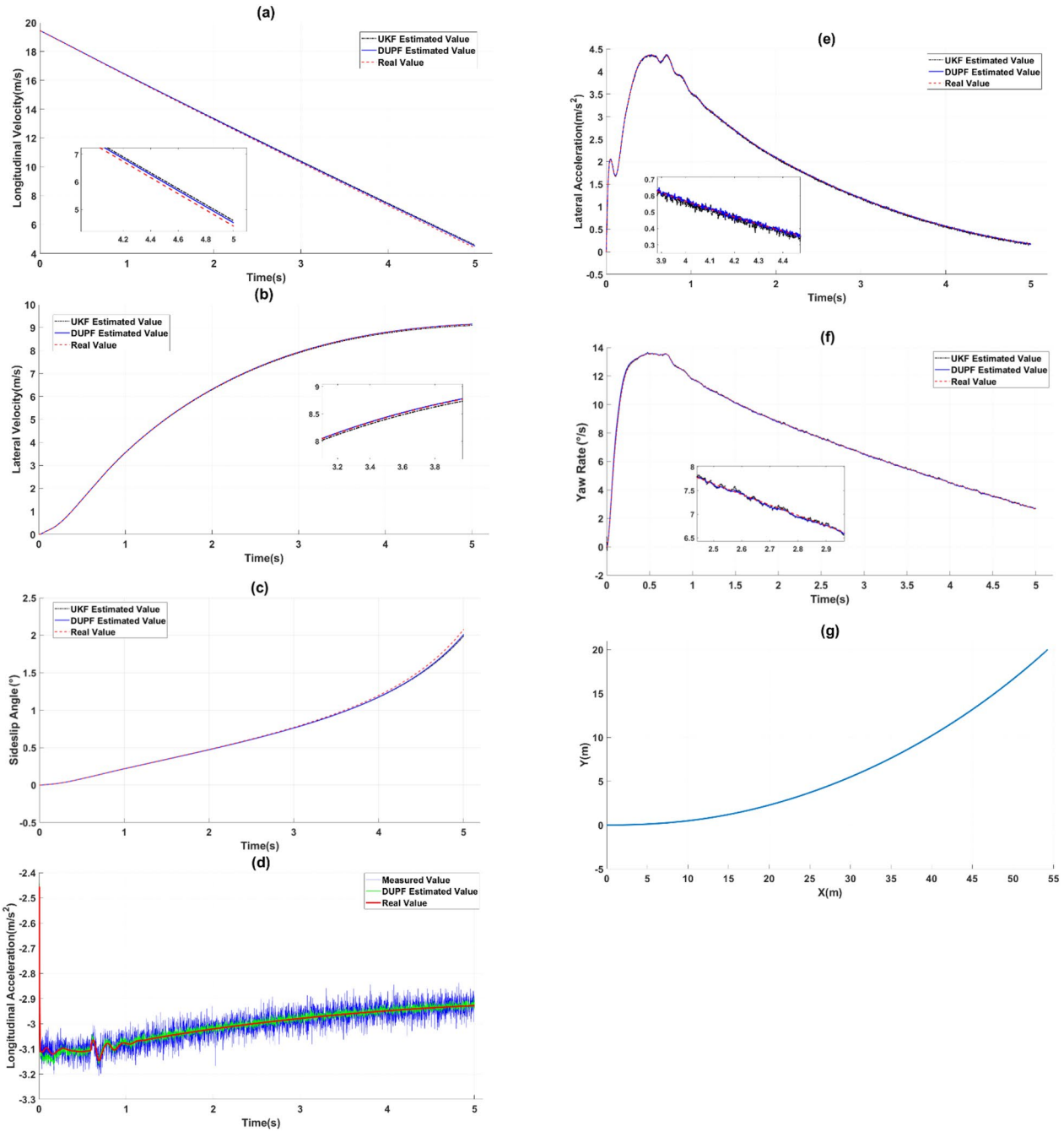

Figure 7 DUPF algorithm estimation result in cornering brake test: (**a**) Longitudinal velocity, (**b**) Lateral velocity, (**c**) Vehicle sideslip angle, (**d**) Longitudinal acceleration, (**e**) Lateral acceleration, (**f**) Yaw rate, (**g**) Driving path

the vehicle state estimation problem under various driving conditions of the vehicle.

4.4 Driving Simulator Test

A simulator test is designed to evaluate the DUPF algorithm. The simulator test platform is constructed by CarSimRT, MATLAB/Simulink and dSPACE. After the NI-PXI receives the acceleration, braking, and steering signals controlled by the driver, it processes and analyzes

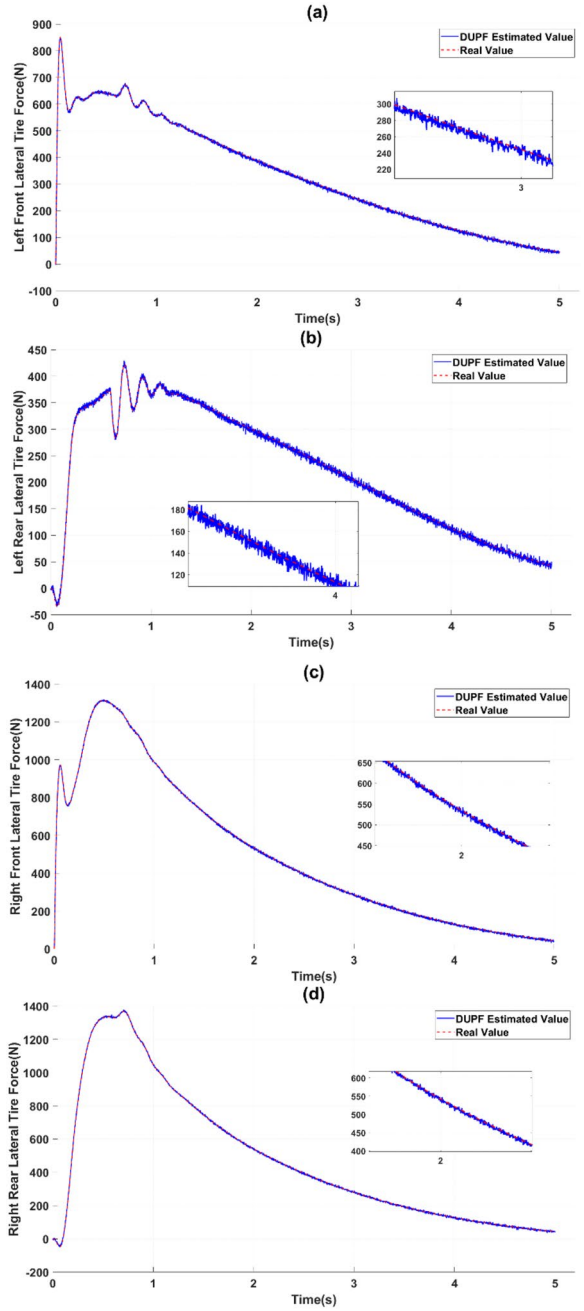

Figure 8 DUPF algorithm estimation result in cornering brake test: (**a**) Left front lateral tire force, (**b**) Left rear lateral tire force, (**c**) Right front lateral tire force, (**d**) Right rear lateral tire force

the signals to obtain the torque input and steering angle input of each wheel, which are transmitted to the vehicle model in CarSim. The sensor signal output in CarSim is subsequently processed by the state observer to obtain the vehicle state information. The real-time video is transmitted back to the display.

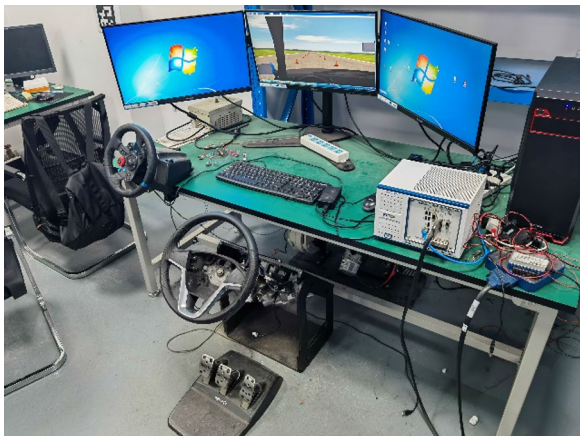

Figure 9 Schematic diagram of online simulation of driving simulator

Figure 9 shows an online simulation of a driving simulator to verify the DUPF algorithm. The driving simulator test adopted a DLC, with the coefficient of road adhesion set as 0.85. The sampling time period is 0–19 s, with a sampling time of 0.02 s, the number of particles is set to 50.

It can be seen from Figure 10 that in the longitudinal direction, the estimation result of the longitudinal acceleration is accurate, while the estimation result of the longitudinal velocity has a certain deviation from the true value of the sensor between 12 and 19 s; in the lateral direction, the estimation result of lateral acceleration is also accurate, and the estimation result has some deviations from the true value of the sensor in 14–19 s, and the estimation result of the yaw rate is accurate. The main reason for the deviation between the longitudinal velocity and the lateral velocity and the true value is: In the process of solving the velocity, there is a certain integral error. However, this part is not within the scope of the algorithm design.

It can be obtained from Figure 11 that the estimation result of tire lateral force obtained by the DUPF algorithm proposed in this paper has real-time performance.

5 Conclusions

(1) A vehicle state estimator based on the DUPF algorithm was proposed to reduce the uncertainty of parameters and the influence of model parameter changes during driving on the estimation results. The algorithm leverages the advantages of the drive-by-wire chassis vehicle that the four-wheel

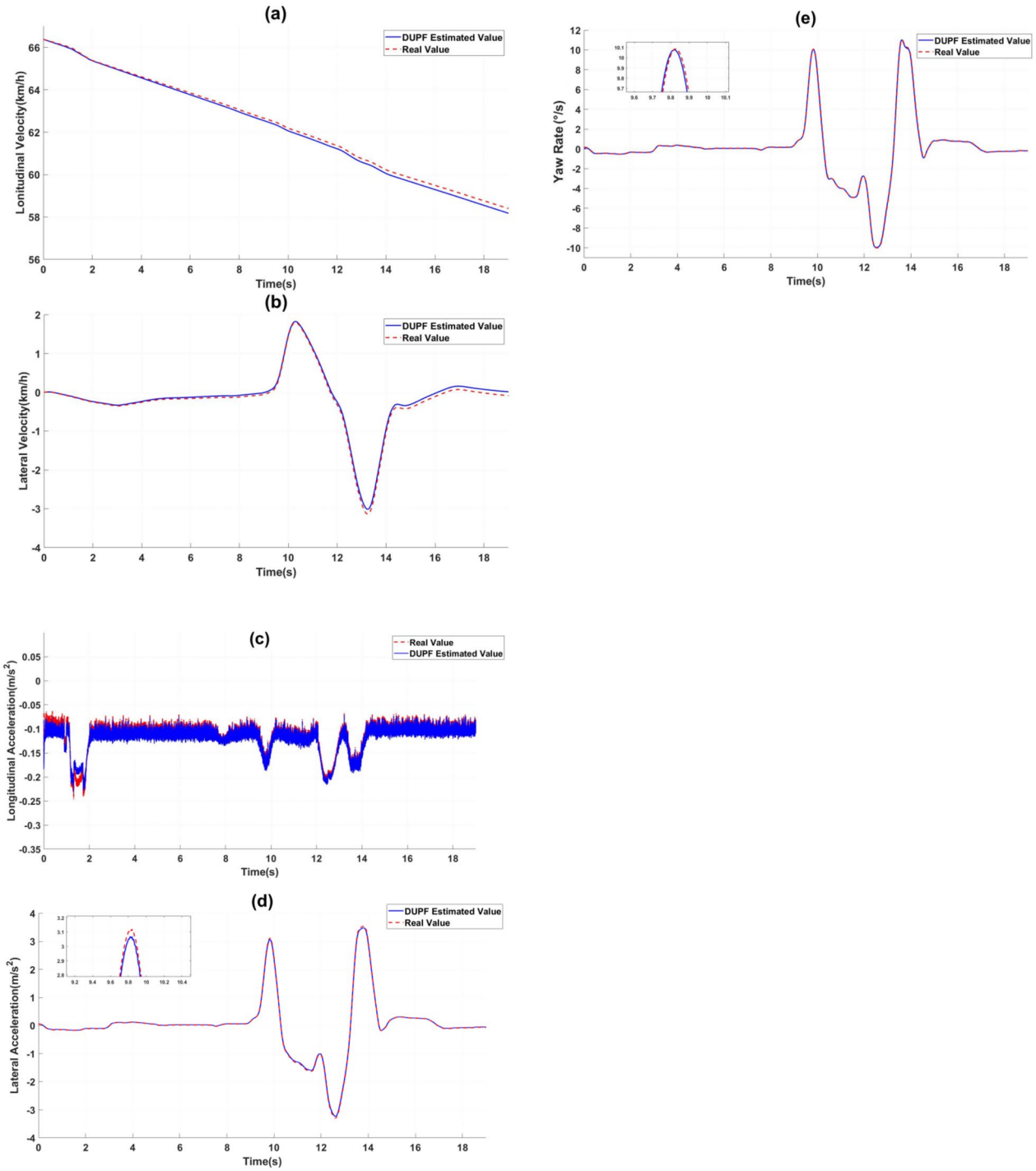

Figure 10 DUPF algorithm estimation result in driving simulator test: (**a**) Longitudinal velocity, (**b**) Lateral velocity, (**c**) Longitudinal acceleration, (**d**) Lateral acceleration, (**e**) Yaw rate

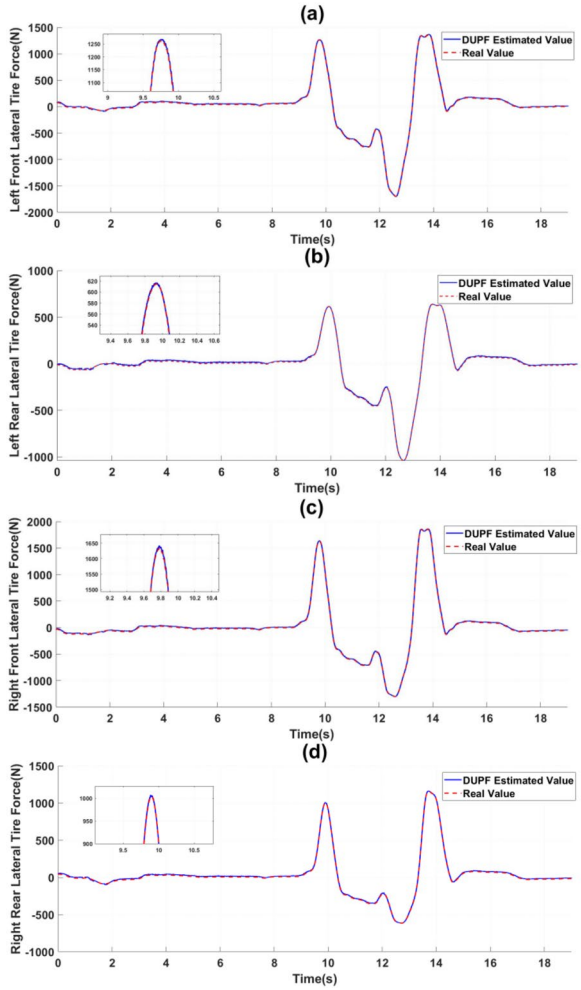

Figure 11 DUPF algorithm estimation result in driving simulator test: (**a**) Left front lateral tire force, (**b**) Left rear lateral tire force, (**c**) Right front lateral tire force, (**d**) Right rear lateral tire force

drive torque and four-wheel steering angle are independently controllable and measurable.

(2) With sets of experiments, DLC, weave test and cornering brake condition and the DUPF algorithm show a good performance, and a good agreement is found between the estimated value curves and actual value curves.

(3) By comparing the TASE of DUPF algorithm with UKF algorithm, the performance of DUPF algorithm has more than 15.88% advantage.

(4) The effectiveness of the DUPF algorithm is verified by driving simulator test.

Acknowledgements
Not applicable.

Authors' Contributions
ZW and HZ were in charge of the whole trial; ZW wrote the manuscript; CC and QJ assisted with sampling and laboratory analyses. All authors read and approved the final manuscript.

Funding
Supported by National Key Research and Development Program of China (Grant No. 2021YFB2500703), Science and Technology Department Program of Jilin Province of China (Grant No. 20230101121JC).

Data availability
The data that support the findings of this study are available on request from the first author, [ZW], upon reasonable request.

Declarations

Competing Interests
The authors declare no competing financial interests.

Received: 20 January 2022 Revised: 28 December 2023 Accepted: 4 January 2024
Published online: 22 February 2024

References

[1] Y Qin, X Tang, T Jia, et al. Noise and vibration suppression in hybrid electric vehicles: State of the art and challenges. *Renewable and Sustainable Energy Reviews,* 2020, 124: 109782.

[2] K Yang, X Tang, Y Qin, et al. Comparative study of trajectory tracking control for automated vehicles via model predictive control and robust H-infinity state feedback control. *Chinese Journal of Mechanical Engineering,* 2021, 34: 74.

[3] X Tang, J Zhang, X Cui, et al. Multi-objective design optimization of a novel dual-mode power-split hybrid powertrain. *IEEE Transactions on Vehicular Technology,* 2022, 71(1): 282-296.

[4] J Ni, J B Hu, C L Xiang. A review for design and dynamics control of unmanned ground vehicle. *Proceedings of the Institution of Mechanical Engineers, Part D: Journal of Automobile Engineering*, 2021, 235(4): 1084-1100.

[5] Y Suzuki, M Takeda. An overview on vehicle lateral dynamics and yaw stability control systems. *J. Adv. Vehicle Eng.*, 2016, 2(4): 182-190.

[6] N M Enache, M Netto, S Mammar, et al. Driver steering assistance for lane departure avoidance. *Control Engineering Practice*, 2009, 17(6): 642-651.

[7] M Keller, C Haß, A Seewald, et al. A model predictive approach to emergency maneuvers in critical traffic situations. *2015 IEEE 18th International Conference on Intelligent Transportation Systems*, Gran Canaria, Spain, Sept 15-18, 2015: 369-374.

[8] J Wu, Y H Liu, F B Wang, et al. Vehicle active steering control research based on two-DOF robust internal model control. *Chinese Journal of Mechanical Engineering*, 2016, 29(4): 739-746.

[9] C F Zong, Z Pan, D Hu, et al. Information fusion algorithm for vehicle state estimation based on extended Kalman filtering. *Journal of Mechanical Engineering*, 2009, 45(10): 272-277. (in Chinese)

[10] C F Zong, D Hu, X Yang, et al. Vehicle driving state estimation based on extended Kalman filter. *Journal of Jilin University (Engineering and Technology Edition)*, 2009, 39(1): 7-11. (in Chinese)

[11] Z G Zhao, H J Chen, J Yang, et al. Estimation of the vehicle speed in the driving mode for a hybrid electric car based on an unscented Kalman filter. *Proceedings of the Institution of Mechanical Engineers, Part D: Journal of Automobile Engineering*, 2015, 229(4): 437-456.

[12] Q J Cui, R J Ding, B Zhou, et al. Path-tracking of an autonomous vehicle via model predictive control and nonlinear filtering. *Proceedings of the Institution of Mechanical Engineers, Part D: Journal of Automobile Engineering*, 2018, 232(9): 1237-1252.

[13] B Zhang, W Z Zhao, S C Zou, et al. A reliable vehicle lateral velocity estimation methodology based on SBI-LSTM during GPS-outage. *IEEE Sensors Journal*, 2020, 21(14): 15485-15495.

[14] B Y Zhang, T Xu, H Wang, et al. Vertical tire forces estimation of multi-axle trucks based on an adaptive treble extend Kalman filter. *Chinese Journal of Mechanical Engineering*, 2021, 34: 55.
[15] B Lenzo, R D Castro. Vehicle sideslip estimation for four-wheel-steering vehicles using a particle filter. *The IAVSD International Symposium on Dynamics of Vehicles on Roads and Tracks*, Gothenburg, Sweden, Aug 12-16, 2019: 1624-1634
[16] K Bogdanski, M C Best. Kalman and particle filtering methods for full vehicle and tyre identification. *Vehicle System Dynamics*, 2018, 56(5): 769-790.
[17] N Y Ko, T G Kim. Comparison of Kalman filter and particle filter used for localization of an underwater vehicle. *2012 9th international conference on ubiquitous robots and ambient intelligence (URAI)*, Daejeon, Korea (South), Feb 26-28, 2013: 350-352.
[18] G F Tong, Z Fang, X H Xu. A particle swarm optimized particle filter for nonlinear system state estimation. *2006 IEEE International Conference on Evolutionary Computation*, Vancouver, BC, Sep 16-21, 2006: 438-442.
[19] K Berntorp. Particle filter for combined wheel-slip and vehicle-motion estimation. *2015 American Control Conference (ACC)*, Jul 1-3, 2015: 5414-5419.
[20] D Y Liu, S Huang, S Wu, et al. Direct yaw-moment control of electric vehicle with in-wheel motor drive system. *International Journal of Automotive Technology*, 2020, 21(4): 1013-1028.
[21] M Lin, J Yoon, B Kim. Self-driving car location estimation based on a particle-aided unscented Kalman filter. *Sensors*, 2020, 20(9): 2544.
[22] Y H Liu, T Li, Y Y Yang, et al. Estimation of tire-road friction coefficient based on combined APF-IEKF and iteration algorithm. *Mechanical Systems and Signal Processing*, 2017, 88: 25-35.
[23] Y T Song, H Y Shu, X B Chen. Chassis integrated control for 4WIS distributed drive EVs with model predictive control based on the UKF observer. *Science China Technological Sciences*, 2020, 63(3): 397-409.
[24] W B Chu, Y G Luo, Y F Dai, et al. In–wheel motor electric vehicle state estimation by using unscented particle filter. *International Journal of Vehicle Design*, 2015, 67(2): 115-136.
[25] J J Zhu, Z P Wang, L Zhang, et al. State and parameter estimation based on a modified particle filter for an in-wheel-motor-drive electric vehicle. *Mechanism and Machine Theory*, 2019, 133: 606-624.
[26] X F Pei, Z F Chen, B Yang, et al. Estimation of states and parameters of multi-axle distributed electric vehicle based on dual unscented Kalman filter. *Science progress*, 2019, 103(1): 1-20.
[27] Z P Wang, J Y Wu, L Zhang, et al. Vehicle sideslip angle estimation for a four-wheel-independent-drive electric vehicle based on a hybrid estimator and a moving polynomial Kalman smoother. *Proceedings of the Institution of Mechanical Engineers, Part K: Journal of Multi-body Dynamics*, 2018, 233(1): 125-140.
[28] H Pacejka. *Tire and vehicle dynamics*. Elsevier, 2005.
[29] Y L Huang, Y G Zhang, N Li, et al. Design of Gaussian approximate filter and smoother for nonlinear systems with correlated noises at one epoch apart. *Circuits, Systems, and Signal Processing*, 2016, 35(11): 3981-4008.

Zixu Wang born in 1999, is currently a master candidate at *State Key Laboratory of Automotive Simulation and Control, Jilin University, China*. Tel: +86-18343526155; E-mail: 345197599@qq.com

Chaoning Chen born in 1999, is currently a Ph.D. candidate at *State Key Laboratory of Automotive Simulation and Control, Jilin University, China.* E-mail:1176660329@qq.com.

Quan Jiang born in 1997, is currently a master candidate at *State Key Laboratory of Automotive Simulation and Control, Jilin University, China.* E-mail:1049819809@qq.com

Hongyu Zheng born in 1980, received the B.E. degree in mechanical engineering and automation and Ph.D. degree in vehicle engineering from *Jilin University, China,* in 2003 and 2009, respectively. From October 2017 to October 2018, he was a visiting research scholar at *Department of Mechanical and Aerospace Engineering, The Ohio State University, USA*. He is currently a professor at *State Key Laboratory of Automotive Simulation and Control, Jilin University, China.* His research interests include vehicle dynamics and control and control of autonomous vehicles. E-mail: zhenghy@jlu.edu.cn

Chuyo Kaku received the M.S. degree in automotive engineering from *Jilin University, China,* in 1988, and the Ph.D. degree in mechanical engineering from *Tokyo Institute of Technology, Japan*, in 1998. From 1988 to 2005, he was an associate professor at *Department of Automotive Engineering, Harbin Institute of Technology, China*. From 1998 to 2016, he worked in engineering field at *Hino Motor Company Ltd., Siemens Automotive JapanToyota Motor Company Ltd., Bosch, Japan*. He is currently working at *Jiangsu Chaoli Electric Company Ltd., China*, with responsibility as the head of the technical center and the chief technology manager. He has been working on the chassis dynamics control projects over 30 years, and achieved more than 20 paper publications and patent certifications. E-mail:guo.kaku@chaoli-electric.com